

AD-A236 525



NASA Contractor Report 187551

ICASE Report No. 91-35

DTIC
ELECTE
JUN 07 1991
S C D

(2)

ICASE

**IGNITION AND STRUCTURE OF A LAMINAR
DIFFUSION FLAME IN A COMPRESSIBLE MIXING
LAYER WITH FINITE RATE CHEMISTRY**

**C. E. Grosch
T. L. Jackson**

Contract No. NAS1-18605
April 1991

Institute for Computer Applications in Science and Engineering
NASA Langley Research Center
Hampton, Virginia 23665-5225

Operated by the Universities Space Research Association



National Aeronautics and
Space Administration

Langley Research Center
Hampton, Virginia 23665-5225

91 6 4 065

DISTRIBUTION STATEMENT A

Approved for public release;
Distribution Unlimited

91-01186



IGNITION AND STRUCTURE OF A LAMINAR DIFFUSION FLAME IN A COMPRESSIBLE MIXING LAYER WITH FINITE RATE CHEMISTRY

C.E. Grosch

Department of Oceanography and
Department of Computer Science
Old Dominion University
Norfolk, Virginia 23529

T.L. Jackson

Department of Mathematics and Statistics
Old Dominion University
Norfolk, Virginia 23529



A-1

Abstract. In this paper we consider the ignition and structure of a reacting compressible mixing layer using finite rate chemistry lying between two streams of reactants with different freestream speeds and temperatures. Numerical integration of the governing equations show that the structure of the reacting flow can be quite complicated depending on the magnitude of the Zeldovich number. In particular, for sufficiently large Zeldovich number, the three regimes first described by Linan and Crespo (1976); i.e., ignition, deflagration, and diffusion flame, occur in supersonic as well as in subsonic flows. An analysis of both the ignition and diffusion flame regimes is presented using a combination of large Zeldovich number asymptotics and numerics. This allows us to analyze the behavior of these regimes as a function of the parameters of the problem. For the ignition regime, a well defined ignition point will always exist provided the adiabatic flame temperature is greater than either freestream temperature. One important result is that at supersonic speeds ignition occurs far downstream from the plate and, as the flow is accelerated to hypersonic speeds, ignition is exponentially delayed. For the diffusion flame regime, the location of the flame changes significantly with changes in the equivalence ratio and the Schmidt numbers.

This work was supported, in part, by the National Aeronautics and Space Administration under NASA Contract No. NAS1-18605 while the authors were in residence at the Institute for Computer Applications in Science and Engineering, NASA Langley Research Center, Hampton, VA 23665.

1. Introduction. Quite recently it has been realized that an understanding of the structure and the stability characteristics of compressible, particularly supersonic, reacting mixing layers is extremely important in the context of the scramjet engine. We have begun a systematic study (Jackson and Grosch, 1990) of the inviscid spatial stability problem of these flows with the combustion zone modeled by the flame sheet, as described by Jackson and Hussaini (1988). We found that the addition of combustion in the form of a flame sheet had important, and complex, effects on the flow stability. In addition, we also showed that with sufficient heat in the flame sheet the flow can undergo a transition from convective to absolute instability, even without the presence of a region of reversed flow in the layer. There are of course situations in which the flame sheet model may not be a sufficiently accurate representation of the combustion process. This could be important in the calculation of the stability characteristics of the reacting flow. Therefore in this paper we return to the problem of determining the structure of the laminar diffusion flame in a compressible, particularly supersonic, mixing layer in using finite rate chemistry.

In a seminal paper, Linan and Crespo (1976) examined the structure of a diffusion flame in the unsteady mixing of two half spaces of fuel and oxidizer. By using a combination of large activation energy asymptotics and numerics they showed that three laminar regimes exist within the flow, the ignition, deflagration, and diffusion regimes. These same regimes were also found by Jackson and Hussaini (1988) in their study of combustion occurring between two parallel supersonic streams with nearly the same speed and temperature. These three regimes are shown in Figure 1. The ignition regime is a region where the combustible gases mix until, at some finite distance downstream of the plate, a thermal explosion occurs and the gas is ignited. The second regime is the deflagration region. After ignition, a pair of well-defined deflagration waves (or "premixed flamelets") emerge according to classical thermal explosion theory. These waves penetrate the mixing layer until all of the deficient reactant is consumed. Just downstream of the deflagration wave, a diffusion flame regime exists where the mixing process is governed by diffusion in the direction normal to the flame. This regime covers the bulk of the overall flow field. Collectively, the ignition and deflagration regimes can occupy a very small portion of the flow field, especially at supersonic speeds. These regimes are highly nonlinear and hence are not easily amenable to analysis. If the incoming flow were turbulent rather than laminar, we surmise there would be a collection of initially discrete premixed flamelets. Full numerical solutions, based on the compressible Navier Stokes equations, appear to miss the ignition and the deflagration regimes, and hence, the premixed flamelet is not captured. Perhaps careful fine-tuning of the numerics will uncover these regimes.

The spatial development of the reacting compressible mixing layer is considered here without making the assumption of infinite Damkohler number. If the Damkohler number were to be taken to be infinite, the flow and combustion fields could be described by similarity solutions. With a finite Damkohler number, the flow and combustion fields evolve in the downstream direction and only approach the similarity solutions of the flame sheet at infinite distance from the plate. The mean fields with finite Damkohler number will, in a future paper, be used in stability calculations.

In the next section we formulate the problem. Numerical solutions to the full equations are then given in section 3. Sections 4 and 5 present an analysis of the ignition and diffusion flame regimes using a combination of large activation energy (and hence Zeldovich number) asymptotics and numerics. Conclusions are then given in the final section.

2. Formulation of the Mean Flow Equations. The nondimensional equations governing the steady two dimensional flow of a compressible, reacting mixing layer with zero pressure gradient lying between streams of reactants with different speeds and temperatures (Figure 1) are given by (Williams, 1985)

$$(\rho U)_x + (\rho V)_y = 0, \quad 1 = \rho T, \quad (1a,b)$$

$$\rho(UU_x + VU_y) = (\mu U_y)_y, \quad (1c)$$

$$\rho(UU_x + VT_y) = Pr^{-1}(\mu T_y)_y + (\gamma - 1)M^2\mu U_y^2 + \beta \Omega, \quad (1d)$$

$$\rho(UF_{j,x} + VF_{j,y}) = Sc_j^{-1}(\mu F_{j,y})_y - \hat{\beta}_j \Omega, \quad j = 1, 2, \quad (1e)$$

$$\Omega = D \rho F_1 F_2 e^{-Ze/T}. \quad (1f)$$

In these equations, the x axis is along the direction of flow; the y axis is normal to the flow; U and V are the velocity components in the x and y directions, respectively; ρ is the density; T is the temperature; and F_1 and F_2 are the mass fractions, with the reaction assumed to be irreversible and of the Arrhenius type. The viscosity μ is assumed to be a function of temperature. The nondimensional parameters appearing above are the Prandtl number Pr , the Schmidt number $Sc_j = Pr Le_j$ for species j where Le_j is the Lewis number for species j , the Mach number $M = U_\infty / a_\infty$, the Zeldovich number $Ze = E/R T_\infty$ with E the dimensional activation energy and R the universal gas constant, D the Damkohler number defined as the ratio of the characteristic diffusion time scale to the characteristic chemical time scale, β the heat release per unit mass fraction of the reactant, $\hat{\beta}_j$ a parameter involving stoichiometry, and finally γ the specific-heats ratio. The equations were nondimensionalized by the freestream values T_∞ , ρ_∞ , U_∞ , $F_{1,\infty}$ for the temperature, density, velocities and mass fractions, respectively. Lengths are referred to some characteristic length scale of the flow.

The boundary conditions consistent with (1) are

$$T = U = F_1 = 1, \quad F_2 = 0 \quad \text{at } x = 0, y > 0, \quad \text{and } x > 0, y \rightarrow \infty, \quad (2a)$$

$$T = \beta_T, \quad U = \beta_U < 1, \quad F_1 = 0, \quad F_2 = \frac{F_{2,\infty}}{F_{1,\infty}} \equiv (\hat{\beta}_2 / \hat{\beta}_1) \phi^{-1} \quad \text{at } x = 0, y < 0, \quad \text{and } x > 0, y \rightarrow -\infty, \quad (2b)$$

where ϕ is the equivalence ratio defined as the ratio of the mass fraction F_1 in the fast stream to the mass fraction F_2 in the slow stream divided by the ratio of their molecular weights times their stoichiometric coefficients. If $\phi = 1$, the mixture is said to be stoichiometric, if $\phi > 1$ it is F_1 rich, and if $\phi < 1$, it is F_1 lean. If β_T is less than one, the slow gas is relatively cold compared to the fast stream, and if β_T is greater than one it is relatively hot. For what follows we take the stoichiometric parameter $\hat{\beta}_j$ to be unity.

The mean flow equations (1) are first transformed into the incompressible form by means of the Howarth-Dorodnitsyn transformation

$$Y = \int_0^y \rho dy, \quad \hat{V} = \rho V + U \int_0^y \rho_x dy. \quad (3)$$

Next we transform to

$$\eta - \eta_0 = \frac{Y}{2 \sqrt{x}} \quad (4)$$

which is the similarity variable for the chemically frozen heat conduction problem, and η_0 corresponds to a shift in the origin. For the case of both streams being supersonic, η_0 is determined uniquely by a compatibility condition found by matching the pressure across the mixing layer, resulting in

$$\frac{1}{\sqrt{M^2 - 1}} V(x, \infty) = \frac{-1}{\sqrt{M^2 \beta_U^2 \beta_T^{-1} - 1}} \frac{\beta_U}{\beta_T} V(x, -\infty),$$

which reduces to that given by Ting (1959) for $\beta_T = 1$. We note here that if the freestream velocities were subsonic, then the compatibility condition would be trivially satisfied, and thus η_0 would remain indeterminate (Klemp and Acrivos, 1972). Under these transformations, with $U = f'(\eta)$ and $\hat{V} = (\eta f' - f) \sqrt{x}$, equation (1) become

$$f''' + 2ff'' = 0, \quad (5a)$$

$$4x f' T_x - Pr^{-1} T'' - 2fT' - (\gamma - 1) M^2 (f'')^2 = 4x \beta D F_1 F_2 e^{-\gamma T}, \quad (5b)$$

$$4x f' F_{j,x} - Sc_j^{-1} F_j'' - 2fF_j' = -4x D F_1 F_2 e^{-\gamma T}, \quad (5c)$$

where the primes indicates partial differentiation with respect to the similarity variable η , and we have assumed the linear viscosity law $\mu = T$ (for Chapman's linear law $\mu = CT$, the constant C can be scaled out by rescaling η and f appropriately, but must be borne in mind when transforming the variables back to their dimensional forms). In terms of the transformed variables, the boundary conditions are

$$T = f' = F_1 = 1, \quad F_2 = 0 \quad \text{at } x = 0, \eta > 0, \quad \text{and } x > 0, \eta \rightarrow \infty, \quad (6a)$$

$$T = \beta_T, \quad f' = \beta_U, \quad F_1 = 0, \quad F_2 = \Phi^{-1} \quad \text{at } x = 0, \eta < 0, \quad \text{and } x > 0, \eta \rightarrow -\infty. \quad (6b)$$

Finally, we note that the Damkohler number D can be scaled out of the equations by a rescaling of the x coordinate. Thus, the Damkohler number is not a true parameter of the above system. However, rescaling x by the Damkohler number is not particularly useful. Since D is typically exponentially large the rescaled coordinate will be exponentially stretched, and this is not desirable from a numerical viewpoint.

3. Numerical Solutions. The system (5) with boundary conditions (6) must be solved numerically. Noting that f is only a function of η , we see that (5b,c) are parabolic in x and thus can be solved by a marching procedure in x . We do this by a Crank-Nicolson procedure. This leads to an implicit nonlinear

system of equations in η which must be solved at each x step. These are solved by an iterative scheme using the boundary conditions in η as given in (6).

In Figure 2a we plot the maximum temperature in η versus x for $Ze = 10$, $M = \beta_U = 0$, $\beta_T = \beta = \phi = 1$. The adiabatic flame temperature is 1.5 for these conditions (see equation (50)), and is larger than either freestream temperature. There is a smooth and gradual transition from the inert solution at $x = 0$ to a diffusion flame. In Figure 2b we show similar results but with $Ze = 30$ and all other parameters the same. Note the sudden transition between the inert solution and the diffusion flame solution occurring in a narrow range in x around $x = 3$. This initial region defines the ignition regime, and hence the flame location. Similar results are shown in Figure 3 but for $M = 2$ with an adiabatic flame temperature of 1.7. From this figure it is apparent that the ignition regime also exists in supersonic flows. As the Mach number increases there is a corresponding increase in the inert temperature at $x = 0$ due to viscous heating, thus lessening the relative effect of combustion on the overall temperature field.

In Figure 4 we plot the temperature and mass fraction profiles as a function of η at various x locations for the same conditions as in Figure 2b. In Figure 4a the rapid rise in the temperature over a narrow range of x should be noted; this indicates ignition. Note also that the temperature peak shifts and that the profile is asymmetric due to the asymmetry in the Lock velocity profile. Figure 4b shows the profile of the F_1 mass fraction. At the smaller values of x , F_1 decreases gradually from 1 at $\eta = +\infty$ to 0 at $\eta = -\infty$, with F_1 varying most rapidly over the range $-3 < \eta < 1$. This shows that there is a diffusion of F_1 from the $\eta \geq 0$ region into the $\eta \leq 0$ region with $F_1 = 0$ only at $\eta = -\infty$. As x is increased the rate of change of F_1 with η over this zone increases. For larger x one can see that F_1 drops to zero for η just below zero showing the presence of a diffusion flame in which all of F_1 is consumed. But note that there is a small secondary maximum in the F_1 distribution in $-3 < \eta < -1$. This shows the presence of a "premixed flamelet" in this premixed region. The distribution of F_2 in η at various x is shown in Figure 4c and is the converse of that of F_1 . The only exception is in the secondary maxima, showing that the presence of the "premixed flamelet" is much more pronounced. Again the asymmetry of the secondary maxima is due to the asymmetry of the velocity profile.

The existence of the "premixed flamelets" and the diffusion flame is shown quite clearly in Figure 5a, where we plot the loci in the (x, η) plane of the maxima of Ω , the chemical production term, also for the data of Figure 2b. As shown in this figure, the position of the maximum decreases from about $\eta = -0.2$ at $x = 0$ to nearly $\eta = -0.6$ at $x \approx 2.9$. The maximum value of Ω increases along this curve. At $x \approx 2.9$ ignition occurs and two maxima appear giving rise to the "premixed flamelets". Beyond the ignition point the premixed flamelets move outwards in the shear layer until all of the deficient reactant is consumed. The appearance of the third maxima just behind the ignition point marks the appearance of the diffusion flame. As x is further increased, the diffusion flame becomes dominant and, as $x \rightarrow \infty$, the diffusion flame thins and approaches a flame sheet characterized by local chemical equilibrium (Jackson & Grosch, 1990). Note that the diffusion flame location is constant in η as x increases.

In Figure 5b we show similar results for the same values of the parameters except that $\beta_T = 0.5$ and $\beta = 1.5$. This case corresponds to unequal freestream temperatures. The adiabatic flame temperature is 1.5 (again see (50)), and is larger than either freestream temperature. Note that the ignition point has moved into the region of higher freestream temperature, and the location of the diffusion flame is unchanged while that of the premixed flames has changed. In Figure 5c we show results for $\beta_T = 0.5$ and $\beta = 0.4$. The

adiabatic flame temperature in this case is 0.95, and is smaller than the freestream temperature at $+\infty$. In contrast to the two previous figures, there is no well defined ignition point; the premixed flame merges smoothly into the diffusion flame whose location is unchanged. In addition, the premixed flamelets are absent. Finally, we note that the behaviour described in Figure 5 also occurs for Mach numbers greater than zero.

In the following two sections, an analysis of the ignition regime and a brief discussion of the diffusion flame regime is given using a combination of large activation energy (and hence Zeldovich number) asymptotics and numerics.

4. Ignition Regime. To investigate the above behaviour analytically for large Zeldovich numbers, we take $Le_j = 1$, $Pr = 1$, resulting in $Sc_j = 1$. This allows us to consider linear combinations of (5b) and (5c) which eliminates the source terms. The solutions of the resulting equations, using the boundary conditions (6), are given by

$$T + \beta F_1 = \beta_T + (1 - \beta_T + \beta) \Psi + \frac{\gamma - 1}{2} M^2 (1 - \beta_U)^2 \Psi (1 - \Psi), \quad (7)$$

$$T + \beta F_2 = \beta_T + \beta \phi^{-1} + (1 - \beta_T - \beta \phi^{-1}) \Psi + \frac{\gamma - 1}{2} M^2 (1 - \beta_U)^2 \Psi (1 - \Psi), \quad (8)$$

where

$$\Psi = \begin{cases} (f' - \beta_U) / (1 - \beta_U) & 0 \leq \beta_U < 1 \\ (1 + \operatorname{erf} \eta) / 2 & \beta_U = 1. \end{cases} \quad (9)$$

Thus F_1 and F_2 can be eliminated from the energy equation (5b), yielding

$$\begin{aligned} 4x f' T_x - T'' - 2f T' - (\gamma - 1) M^2 (1 - \beta_U)^2 (\Psi')^2 \\ = \frac{4x D}{\beta} [\beta_T + (1 - \beta_T + \beta) \Psi + \frac{\gamma - 1}{2} M^2 (1 - \beta_U)^2 \Psi (1 - \Psi) - T] \\ \times [\beta_T + \beta \phi^{-1} + (1 - \beta_T - \beta \phi^{-1}) \Psi + \frac{\gamma - 1}{2} M^2 (1 - \beta_U)^2 \Psi (1 - \Psi) - T] e^{-Z_e T} \end{aligned} \quad (10)$$

for the temperature, subject to the boundary conditions

$$T = 1 \quad \text{at } x = 0, \eta > 0, \quad \text{and } x > 0, \eta \rightarrow \infty, \quad (11a)$$

$$T = \beta_T \quad \text{at } x = 0, \eta < 0, \quad \text{and } x > 0, \eta \rightarrow -\infty. \quad (11b)$$

In the absence of chemistry, equation (10) reduces to

$$4x f' T_x - T'' - 2f T' - (\gamma - 1) M^2 (1 - \beta_U)^2 (\Psi')^2 = 0, \quad (12)$$

which possesses the inert similarity solution

$$T_I \equiv T_I(\eta) = 1 - (1 - \beta_T)(1 - \Psi) + \frac{\gamma - 1}{2} M^2 (1 - \beta_U)^2 \Psi (1 - \Psi), \quad (13)$$

which is also a solution of (10) for small x . As x increases, more of the combustible mixes until, at some finite distance downstream of the plate, a thermal explosion occurs characterized by significant departure from the inert.

To analyze the ignition process, we expand about the inert by defining T_1

$$T_1 = Ze (T - T_I), \quad (14)$$

and take the asymptotic limit $Ze \rightarrow \infty$. Substituting into (10), we see that the left hand side becomes $O(Ze^{-1})$ while the right hand side is $O(D e^{-Ze/T_*})$, where $T_* = \max(T_I)$. In order to balance these terms, D must therefore have the form

$$D = \frac{\phi}{\beta \delta Ze} e^{Ze/T_*}, \quad (15)$$

where δ will be chosen in the course of the analysis. Substituting (14) and (15) into (10) yields the following equation for T_1

$$\begin{aligned} 4x T_{1,x} - T_1'' - 2f T_1' &= 4x \frac{\phi}{\delta \beta^2} [\beta \Psi - Ze^{-1} T_1] \\ &\times [\beta \phi^{-1} (1 - \Psi) - Ze^{-1} T_1] \exp \left[\frac{T_1 + Ze (T_I - T_*)}{T_* (T_I + Ze^{-1} T_1)} \right], \end{aligned} \quad (16)$$

which must be solved subject to the boundary conditions

$$T_1 = 0 \quad \text{at} \quad x = 0 \quad \text{and at} \quad \eta \rightarrow \pm \infty. \quad (17)$$

Note that the right hand side of (16) is exponentially small except where $|T_I - T_*| = O(Ze^{-1})$. There are now several cases to consider, depending upon the magnitude of the parameters β_T , β_U , and M . Each case is described below.

4.1. $|1 - \beta_T| \ll 1$, $|1 - \beta_U| \ll 1$, and $M = O(1)$.

This case corresponds to the simple but important case of ignition for nearly equal freestream temperatures and velocities, and the analysis is presented by Jackson and Hussaini (1988). For this reason, we only briefly review the results here. We begin by setting

$$\beta_T = Ze (1 - \beta_T), \quad \beta_U = \sqrt{Ze} (1 - \beta_U), \quad (18)$$

with β_T , β_U , and M fixed and $O(1)$. In particular, we see that

$$f = \eta + O(Ze^{-1/2}), \quad \Psi = \Psi_o + O(Ze^{-1/2}), \quad \Psi_o = \frac{1}{2}(1 + \operatorname{erf} \eta). \quad (19)$$

The inert solution (13) is expanded as

$$T_I = 1 + Ze^{-1}[-\beta_T(1 - \Psi_o) + \frac{\gamma-1}{2}M^2\beta_U^2\Psi_o(1 - \Psi_o)] + O(Ze^{-2}), \quad (20)$$

which yields $T_* = 1$. Substituting into (16), together with the choice $\delta = 1$, yields the following equation for the disturbance temperature

$$4x T_{1,x} - 2\eta T_{1,\eta} - T_{1,\eta\eta} = 4x \Psi_o(1 - \Psi_o) \exp\left[T_1 - \beta_T(1 - \Psi_o) + \frac{\gamma-1}{2}M^2\beta_U^2\Psi_o(1 - \Psi_o)\right], \quad (21)$$

subject to the boundary conditions (17). This equation was solved numerically by a Crank-Nicolson implicit scheme. As x increases, the solution for T_1 becomes unbounded at some finite location (x_*, η_*) downstream of the plate, indicating thermal runaway. The results are presented in Figure 6, where we plot x_* and η_* as a function of $M\beta_U$ for various values of β_T . Note that for a fixed β_T , increasing $M\beta_U$ causes the ignition point to move closer to the origin. For a fixed $M\beta_U$, increasing (or decreasing) β_T from zero (i.e., cooling (or heating) the gas from below) causes η_* to move into the region of higher freestream temperature. In addition, x_* increases as the gas is cooled below and decreases as the gas is heated below.

As noted above, as β_T increases or decreases from zero, the ignition point moves into the region of higher freestream temperature. This case corresponds to different freestream temperatures, and can be analyzed in the limit $|\beta_T| \rightarrow \infty$. We shall assume $\beta_T < 1$ ($\beta_T > 0$) and hence the ignition point is located in the region $\eta \gg 1$. The analysis for the case $\beta_T > 1$ ($\beta_T < 0$) is similar. Following the analysis of Linan and Crespo (1976), we set

$$\beta_T(1 - \Psi_o) = z, \quad 0 < z < \infty, \quad (22)$$

and using the asymptotic expansion of Ψ_o , we see that

$$\eta^2 = \ln(\beta_T / 2\sqrt{\pi}) - \ln \eta - \ln z. \quad (23)$$

The reaction zone is located where $z = O(1)$, and to a first approximation we get

$$\eta_*^2 = \ln(\beta_T / 2\sqrt{\pi}) - \ln \eta_*, \quad (24)$$

where η_* defines the ignition location. Since the chemistry is confined to a thin region about η_* , we shift to the reaction zone coordinate

$$\eta = \eta_* - \frac{1}{2\eta_*} \ln z. \quad (25)$$

Substitution into (16), together with $T_* = 1$, and neglecting terms of $O(\eta^{-2})$, yields a canonical equation for T_1 . Repeating the analysis for $\beta_T > 1$ yields a canonical equation for T_1 of exactly the same form, the differences being in the definition of the parameters, the flame now being located in the slow stream where the gas is initially hotter, and $T_* = \beta_T$. This canonical equation, originally given by Linan and Crespo (1976) in a different context, is

$$-x_1^{-1} z^2 \psi_{zz} = (z - \Lambda \psi) e^{\psi - z} \quad (26)$$

where

$$x_1 = \begin{cases} x / (\beta_T \eta^2) & \beta_T < 1 \\ x / (-\beta_T \eta^2) & \beta_T > 1, \end{cases} \quad \Lambda = \begin{cases} \phi(1 - \beta_T)/\beta & \beta_T < 1 \\ (\beta_T - 1)/\beta & \beta_T > 1. \end{cases} \quad (27)$$

This equation must be solved subject to the boundary conditions

$$\psi(0) = 0, \quad \psi_z(\infty) = 0. \quad (28)$$

The first boundary condition is a restatement of (17), while the second boundary condition comes from matching with the chemically frozen region $\eta = O(1)$. Note that x is now a parameter of the equation.

Linan and Crespo have shown that for $\Lambda < 1$, ψ is double valued for $x_1 < x_{1*}$, single valued at $x_1 = x_{1*}$, and does not exist for $x_1 > x_{1*}$. Near x_{1*} we note that $\partial\psi/\partial x_1$ becomes large showing that the x partial derivative can no longer be neglected in (16). Therefore x_{1*} may be considered as the ignition point. For $\Lambda > 1$, ψ is single valued for all x_1 indicating that there is no well defined ignition point. In this case the premixed flame merges smoothly with the diffusion flame and there are no premixed flamelets. This behaviour is shown numerically in Figure 5c. In Figure 7 we plot the ignition point x_{1*} versus Λ . As Λ approaches one from below, the ignition point moves off to infinity, while for $\Lambda > 1$ there is no well defined ignition point.

4.2. $|1 - \beta_T| \ll 1$, $\beta_T < 1$, and $M \ll 1$.

This case corresponds to nearly equal freestream temperatures in a shear flow at small Mach numbers, and we therefore set

$$\tilde{\beta}_T = Ze(1 - \beta_T), \quad \tilde{M} = \sqrt{Ze} M, \quad (29)$$

with $\tilde{\beta}_T$ and \tilde{M} fixed and $O(1)$. The inert solution (13) is now expanded as

$$T_I = 1 + Ze^{-1} [-\tilde{\beta}_T(1 - \Psi) + \frac{\gamma - 1}{2} \tilde{M}^2(1 - \beta_U)^2 \Psi(1 - \Psi)] + O(Ze^{-2}), \quad (30)$$

again yielding $T_* = 1$. Here, Ψ is given by (9a). Substituting into (16), again with the choice $\delta = 1$, yields the equation for the disturbance temperature

$$4x f' T_{1x} - 2f T_1' - T_1'' = 4x \Psi(1 - \Psi) \exp \left[T_1 - \beta_T(1 - \Psi) + \frac{\gamma - 1}{2} \tilde{M}^2 (1 - \beta_U)^2 \Psi(1 - \Psi) \right], \quad (31)$$

subject to the boundary conditions (17). This equation was again solved by a Crank-Nicolson scheme. As x increases, the solution for T_1 becomes unbounded at some finite location (x_*, η_*) downstream of the plate, indicating thermal runaway. Some results are presented in Figure 8, where we plot x_* and η_* as a function of β_U for various values of \tilde{M} and $\beta_T = 0$. We first note that for $\beta_U = 1$, the ignition point is independent of the Mach number. For a fixed \tilde{M} , decreasing β_U from one causes the ignition point to move back toward the plate and into the slower moving gas. At fixed $\beta_U < 1$, an increase in \tilde{M} causes the ignition point to shift toward the origin.

Increasing or decreasing β_T has the same effect on the ignition location as in the previous case. To see this, we first note that the asymptotic expansion of the Lock profile (9a) for large η is given by

$$f' = \begin{cases} 1 - A(\eta + B)^{-1} \exp(-(\eta + B)^2) & \eta \rightarrow +\infty \\ \beta_U + A(\eta + B)^{-1} \exp(-\beta_U(\eta + B)^2) & \eta \rightarrow -\infty, \end{cases} \quad (32)$$

where A and B are known constants. Following the analysis of the previous section, we again obtain the canonical equation (26) for the temperature perturbation, with x_1 now given by

$$x_1 = \begin{cases} x / (\beta_T(\eta_* + B)^2) & \beta_T < 1 \\ x / (-\beta_T(\eta_* + B)^2) & \beta_T > 1, \end{cases} \quad (33)$$

and A as before.

$$4.3. \quad \beta_T > 0, \quad 0 \leq \beta_U < 1, \quad \text{and} \quad \tilde{M} > 0.$$

For Mach numbers greater than zero, $\beta_U < 1$ and any value of β_T , the inert solution (13) has a maximum at $T_1' = 0$; i.e.,

$$\Psi \left[1 - \beta_T + \frac{\gamma - 1}{2} \tilde{M}^2 (1 - \beta_U)^2 (1 - 2\Psi) \right] = 0. \quad (34)$$

If $\Psi' = 0$, then the location of the reaction zone will occur in the outer region $|\eta| \gg 1$ where the gas is initially hotter. Since the analysis for this case will be similar to that of the previous two cases, we will not present it here. If the second term of (34) is zero, then the reaction zone will occur in the mixing layer, and is given by the implicit relation

$$\Psi_* \equiv \Psi(\eta_*) = \frac{1}{2} + \frac{1 - \beta_T}{(\gamma - 1) \tilde{M}^2 (1 - \beta_U)^2}. \quad (35)$$

The corresponding maximum value of T_I is given by

$$T_* \equiv \max(T_I) = 1 - \frac{1 - \beta_T}{2} + \frac{\gamma - 1}{8} M^2 (1 - \beta_U)^2 + \frac{(1 - \beta_T)^2}{2(\gamma - 1)M^2(1 - \beta_U)^2}. \quad (36)$$

Substituting (34-36) into (16) shows that the right hand side of (16) is exponentially small except in a narrow region where $|T_I - T_*| \approx O(Ze^{-1})$. Outside this region the equation is essentially frozen, and is given by

$$4x T_{1,x} = T_1'' + 2f T_1', \quad (37)$$

valid on either side of the reaction zone. To study the structure of the reaction zone we define the new coordinate

$$\eta = \eta_* + \delta z, \quad (38)$$

where δ is the thickness of the reaction zone and is not yet specified. The temperature and velocity are also expanded as

$$T_1 = T_{1*}(x) + \delta T_{11}(x, \eta) + \dots, \quad \Psi = \Psi_* + \delta z \Psi_*' + \dots, \quad (39)$$

Substitution into (16) yields

$$\frac{d^2 T_{11}}{dz^2} = -4x \Psi_* (1 - \Psi_*) \exp \left[\frac{T_{1*} - \frac{\gamma - 1}{2} M^2 (1 - \beta_U)^2 (\Psi_*')^2 z^2}{T_*^2} \right], \quad (40)$$

where we have chosen $\delta = Ze^{-1/2}$. Note that (40) can be integrated once to yield

$$\frac{dT_{11}}{dz} = -d(x) \int_{-\infty}^z \frac{b}{\sqrt{\pi}} \exp[-b^2 z^2] dz + c_1(x), \quad (41)$$

where

$$d(x) = 4x \Psi_* (1 - \Psi_*) \exp[T_{1*}/T_*^2] \frac{\sqrt{\pi}}{b}, \quad (42a)$$

$$b^2 = \frac{\gamma - 1}{2} M^2 (1 - \beta_U)^2 (\Psi_*')^2 T_*^{-2}. \quad (42b)$$

Evaluating (41) at $z = \pm \infty$ yields the matching conditions for (37). Specifically, we now solve (37) subject to the boundary and jump conditions

$$T_1(x, \infty) = 0, \quad T_1(x, \eta^+) = T_{1*}(x), \quad \frac{dT_1}{d\eta}(x, \eta^+) = c_1(x) - d(x), \quad (43)$$

$$T_1(x, -\infty) = 0, \quad T_1(x, \eta^-) = T_{1*}(x), \quad \frac{dT_1}{d\eta}(x, \eta^-) = c_1(x), \quad (44)$$

with the initial conditions

$$T_1(0, \eta) = 0, \quad \eta \neq \eta_*, \quad (45)$$

Equation (37), valid on either side of the reaction zone, can be solved numerically by marching forward in x . The unknown functions $T_{1*}(x)$ and $c_1(x)$ are chosen at each x location so as to satisfy the boundary conditions at $\eta = \pm\infty$. Thermal runaway will occur at (x_*, η_*) , thus defining the flame location. In Figure 9 we show T_{1*} and c_1 as a function of x for $\beta_T = 0.5$, $\beta_U = 0$, and $M = 2$. Note that as x approaches x_* , T_{1*} becomes unbounded indicating thermal runaway. In Figure 10 we plot the ignition location x_* and η_* as a function of the Mach number for $\beta_U = 0$ and various values of β_T . As the Mach number becomes large x_* moves off to $+\infty$ while η_* tends to zero for any β_T . This shows that in the supersonic region ignition occurs far downstream of the plate and, as the flow is accelerated to hypersonic speeds, ignition is exponentially delayed. For unequal freestream temperatures ($\beta_T \neq 1$), as the Mach number goes to zero then η_* moves out of the mixing layer into the region of higher freestream temperature. When this occurs this analysis is no longer appropriate, and one must consider the case of $\Psi' = 0$ in (34).

5. Diffusion Flame Regime. Typically, a diffusion flame is characterized by a chemical reaction time that is much smaller than a characteristic diffusion time. Chemical reactions then occur in a narrow zone between the fuel and the oxidizer, where the concentrations of both reactants are very small. Mathematically, the assumption of very fast chemical reaction rates leads to the limit of infinite Damkohler number which reduces the diffusion flame to a flame sheet (i.e. local chemical equilibrium). This assumption significantly reduces the complexity of the problem since it eliminates the analysis associated with the chemical kinetics. For many flows, the assumption of local chemical equilibrium adequately predicts the location and the shape of the diffusion flame (Buckmaster and Ludford, 1982; Williams, 1985). Since the flame sheet model has a simple similarity solution and hence is amenable to analysis, we give its structure below. For finite values of the Damkohler number, equations (5b,c) must be solved directly using the numerical scheme mentioned above.

Assuming unit Lewis and Prandtl numbers and a linear viscosity law, the profile associated with the flame sheet model is given by (Jackson and Hussaini, 1988; Jackson and Grosch, 1990)

$$F_1 = 1 - (1 + \phi^{-1})(1 - \Psi), \quad F_2 = 0, \quad (46)$$

$$T = \beta_T + \beta\phi^{-1} + (1 - \beta_T - \beta\phi^{-1})\Psi + \frac{\gamma-1}{2} M^2 (1 - \beta_U)^2 \Psi(1 - \Psi), \quad (47)$$

valid for $\eta > \eta_f$, and

$$F_1 = 0, \quad F_2 = \phi^{-1} - (1 + \phi^{-1})\Psi, \quad (48)$$

$$T = \beta_T + (1 - \beta_T + \beta)\Psi + \frac{\gamma - 1}{2} M^2 (1 - \beta_U)^2 \Psi (1 - \Psi), \quad (49)$$

valid for $\eta < \eta_f$. Here, η_f gives the location of the flame sheet where both the reactants vanish, and T takes the adiabatic flame value

$$T_f = \beta_T + (1 - \beta_T + \beta)\Psi_f + \frac{\gamma - 1}{2} M^2 (1 - \beta_U)^2 \Psi_f (1 - \Psi_f). \quad (50)$$

The flame location is given by the implicit relation

$$\Psi_f \equiv \Psi(\eta_f) = \frac{1}{1 + \phi} \quad (51)$$

which is independent of β_T and M . This is only valid for the case of a linear viscosity law where the momentum equation decouples from the energy equation. For a more general viscosity law, the flame location will depend on β_T and M as well. When using (3) to transform back to the physical coordinates, the diffusion flame location in physical space will depend on β_U , ϕ , β_T and M , independently of the viscosity-temperature relation. The internal structure of the diffusion flame, which appears as a discontinuity on the η scale, is described in in Jackson and Hussaini (1988).

The above assumption of unit Lewis and Prandtl numbers led to a closed-form analytical solution. Since the Prandtl number is about 0.72 and the Lewis numbers are not one, the Schmidt numbers will in general not be one. To determine the influence of the Schmidt numbers on the location of the diffusion flame, we begin by considering (5b,c) in the limit of infinite Damkohler number

$$Pr^{-1} T'' + 2 f T' + (\gamma - 1) M^2 (f'')^2 = 0, \quad (52)$$

$$Sc_j^{-1} F_j'' + 2 f F_j' = 0, \quad (53)$$

valid on either side of the flame sheet. The appropriate boundary and jump conditions are given by

$$T = 1, \quad F_1 = 1, \quad F_2 = 0 \quad \text{as } \eta \rightarrow \infty, \quad (54a)$$

$$[Pr^{-1} T' + \beta Sc_j^{-1} F_j'] = 0, \quad [T] = 0, \quad F_1 = F_2 = 0, \quad \text{at } \eta = \eta_f, \quad (54b)$$

$$T = \beta_T, \quad F_1 = 0, \quad F_2 = \phi^{-1} \quad \text{as } \eta \rightarrow -\infty, \quad (54c)$$

where $[]$ denotes the jump $()_{\eta_f^+} - ()_{\eta_f^-}$ at η_f . Integrating the equations (53) for the mass fractions yields

$$F_1 = 1 - c_1 \int_{\eta}^{\infty} (\Psi')^{Sc_1} d\eta, \quad F_2 = 0, \quad (55)$$

valid for $\eta > \eta_f$, and

$$F_1 = 0, \quad F_2 = \phi^{-1} - c_2 \int_{-\infty}^{\eta} (\Psi')^{Sc_2} d\eta, \quad (56)$$

valid for $\eta < \eta_f$. Using the boundary condition $F_1 = F_2 = 0$ at η_f yields

$$c_1 = \frac{1}{\int_{\eta_f}^{\infty} (\Psi')^{Sc_1} d\eta}, \quad c_2 = \frac{\phi^{-1}}{\int_{-\infty}^{\eta_f} (\Psi')^{Sc_2} d\eta}. \quad (57)$$

The location of the flame sheet η_f , where both reactants vanish simultaneously, is given by the implicit relation

$$\phi Sc_2 \int_{-\infty}^{\eta_f} (\Psi')^{Sc_2} d\eta = Sc_1 (\Psi')^{Sc_2 - Sc_1} \int_{\eta_f}^{\infty} (\Psi')^{Sc_1} d\eta, \quad (58)$$

obtained from the jump condition (54b) on the derivatives. In Figure 11 we plot the flame location as a function of Sc_1 for various cases. In Figure 11a we show the variation with Sc_2 . As Sc_2 increases the flame location moves into the slower moving stream. In Figure 11b we show the variation with the equivalence ratio. As ϕ increases the flame location also moves into the slower moving stream. Finally, in Figure 11c we show the variation with β_U . As β_U increases the flame moves into the faster stream.

6. Conclusions. In this paper we have considered the ignition and structure of a reacting compressible mixing layer using finite rate chemistry lying between two streams of reactants with different freestream speeds and temperatures. Numerical integration of the governing equations show that the structure of the reacting flow can be quite complicated depending on the magnitude of the Zeldovich number. In particular, for sufficiently large Zeldovich number, the three regimes first described by Linan and Crespo (1976); i.e., ignition, deflagration, and diffusion flame, occur in supersonic as well as in subsonic flows. Our numerics pick up the premixed flamelets as clearly shown by the distribution of the production term. Again, depending on the magnitude of the Zeldovich number, there can be a gradual or sudden transition from an inert solution to a diffusion flame.

An analysis of both the ignition and diffusion flame regimes was presented using a combination of large Zeldovich number asymptotics and numerics. This allowed us to analyze the behavior of these regimes as a function of the parameters of the problem. For the ignition regime, a well defined ignition point will always exist provided the adiabatic flame temperature is greater than either freestream temperature. One important result is that at supersonic speeds ignition occurs far downstream from the plate and, as the flow is accelerated to hypersonic speeds, ignition is exponentially delayed. For the diffusion flame regime, the location of the flame changes significantly with changes in the equivalence ratio and the Schmidt numbers.

There are substantial changes in the temperature and mass fraction distribution as the mixing layer evolves downstream. These are expected to have a considerable effect on the stability characteristics of the flow. The changes, and particularly the rate of change, in the mean profiles were shown to be very sensitive

to the value of the Zeldovich number. Therefore we expect that the stability characteristics will also be quite sensitive to the value of the Zeldovich number. The stability calculations are underway and will be reported at a later date.

REFERENCES

- Buckmaster, J.D. & Ludford, G.S.S. (1982) *Theory of Laminar Flames*. Cambridge University Press, Cambridge.
- Jackson, T.L. & Grosch, C.E. (1990) Inviscid Spatial Stability of a Compressible Mixing Layer. Part II. The Flame Sheet Model. *J. Fluid Mech.*, 217, pp. 391-420. 217, pp. 391-420.
- Jackson, T.L. & Hussaini, M.Y. (1988) An Asymptotic Analysis of Supersonic Reacting Mixing Layers. *Comb. Sci. Tech.*, 57, pp. 129-140.
- Klemp, J. B. and Acrivos, A. (1972) A note on the laminar mixing of two uniform parallel semi-infinite streams. *J. Fluid Mech.*, 55, pp. 25-30.
- Linan, A. & Crespo, A. (1976) An asymptotic analysis of unsteady diffusion flames for large activation energies. *Comb. Sci. Tech.*, 14, pp. 95-117.
- Stewartson, K. (1964) *The Theory of Laminar Boundary Layers in Compressible Fluids*. Oxford University Press, Great Britain.
- Ting, L. (1959) On the mixing of two parallel streams. *J. Math. Phys.*, 28, pp. 153-165.
- Williams, F.A. (1985) *Combustion Theory*, 2nd Ed., The Benjamin/Cummings Pub. Co., Menlo Park, CA.

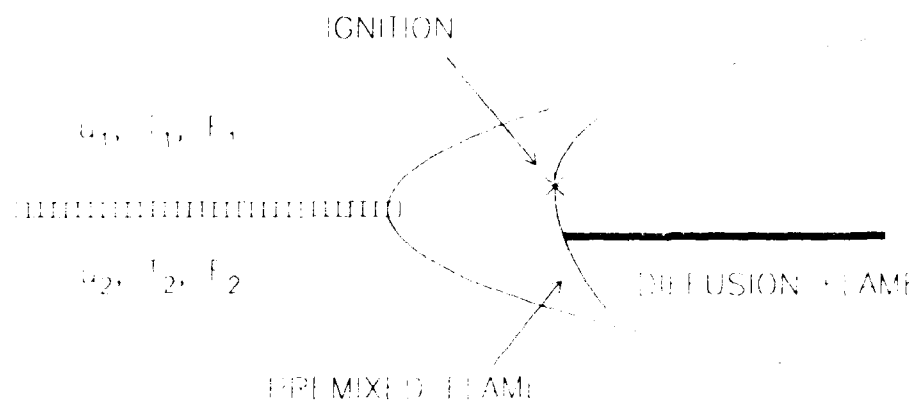


Figure 1. Schematic showing the reacting mixing layer, where the adiabatic flame temperature is greater than T_1 and T_2 .

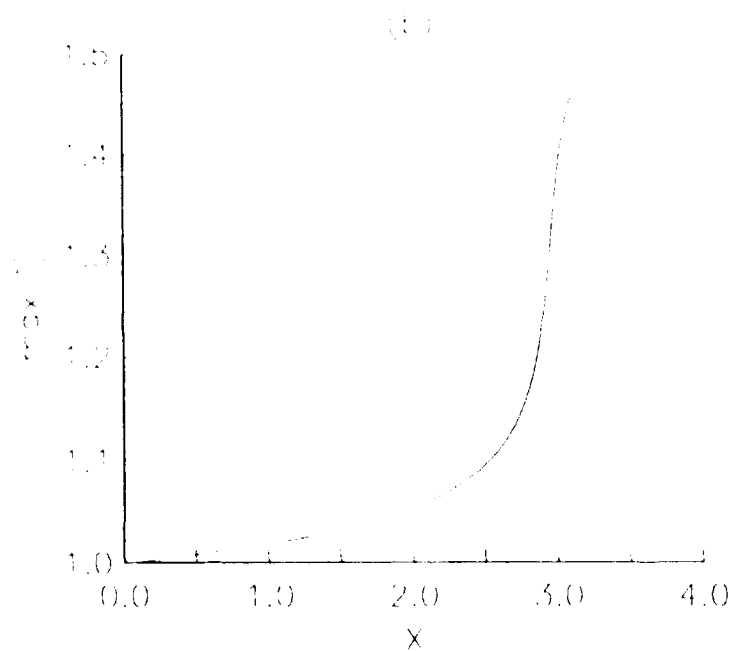
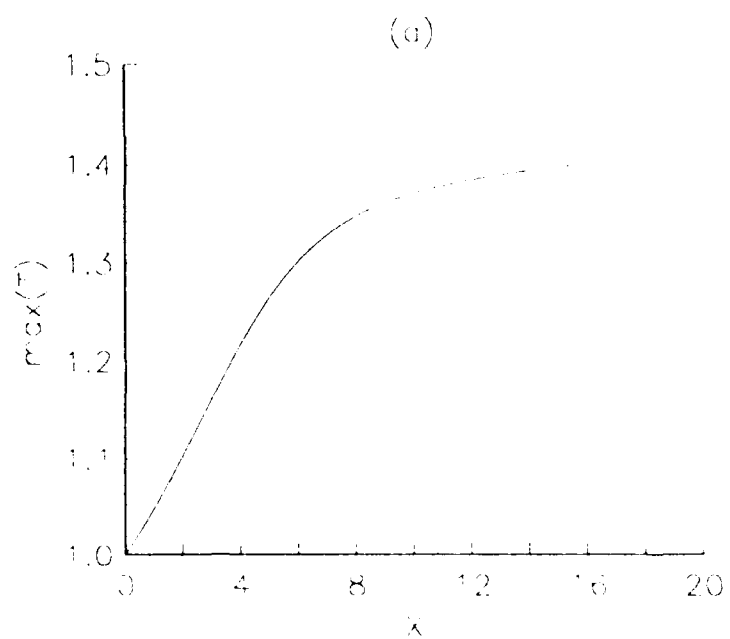


Figure 2. Plot of the maximum temperature in η versus x for $M = \beta_U = 0$, $\beta_T = \beta = \phi = 1$. (a) $Ze = 10$, (b) $Ze = 30$. Here, $D = e^{1/2} / Ze$.

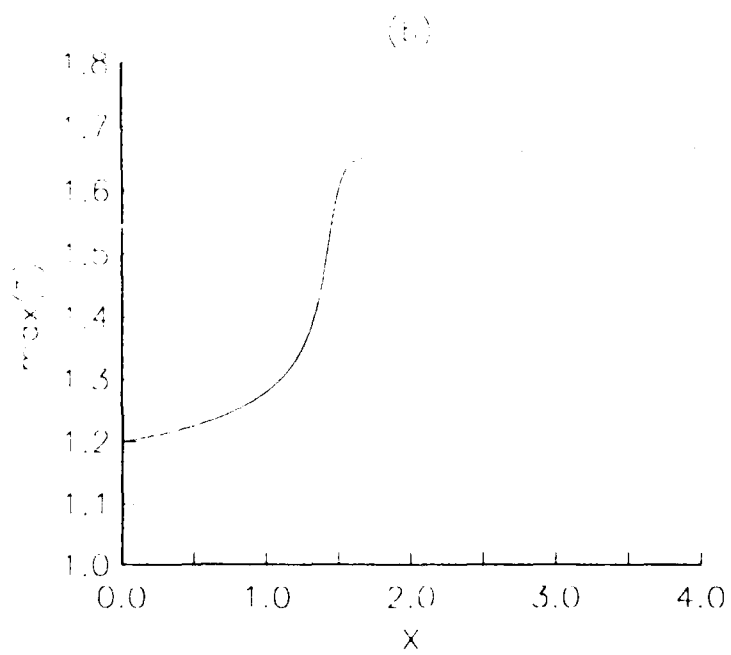
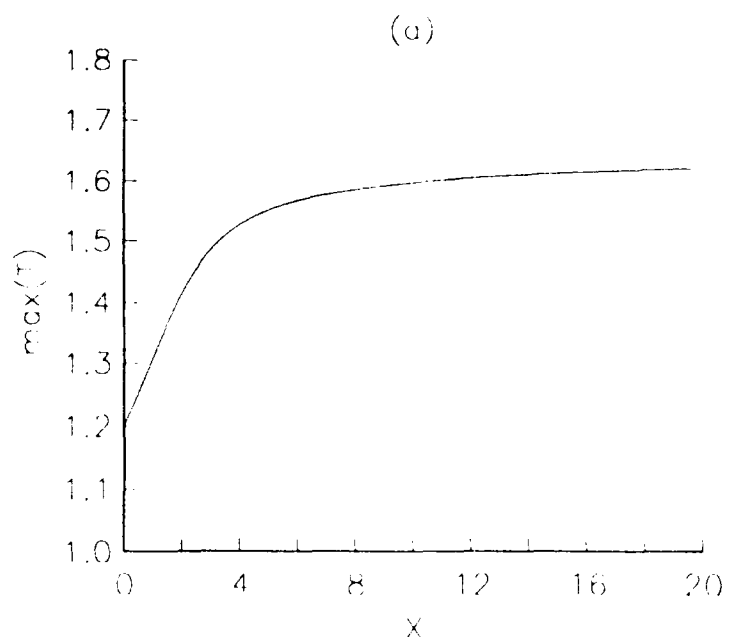


Figure 3. Plot of the maximum temperature in η versus x for $M = 2$, $\beta_U = 0$, $\beta_T = \beta = \phi = 1$. (a) $Ze = 10$, (b) $Ze = 30$. Here, $D = e^{Ze/1.2}/Ze$.

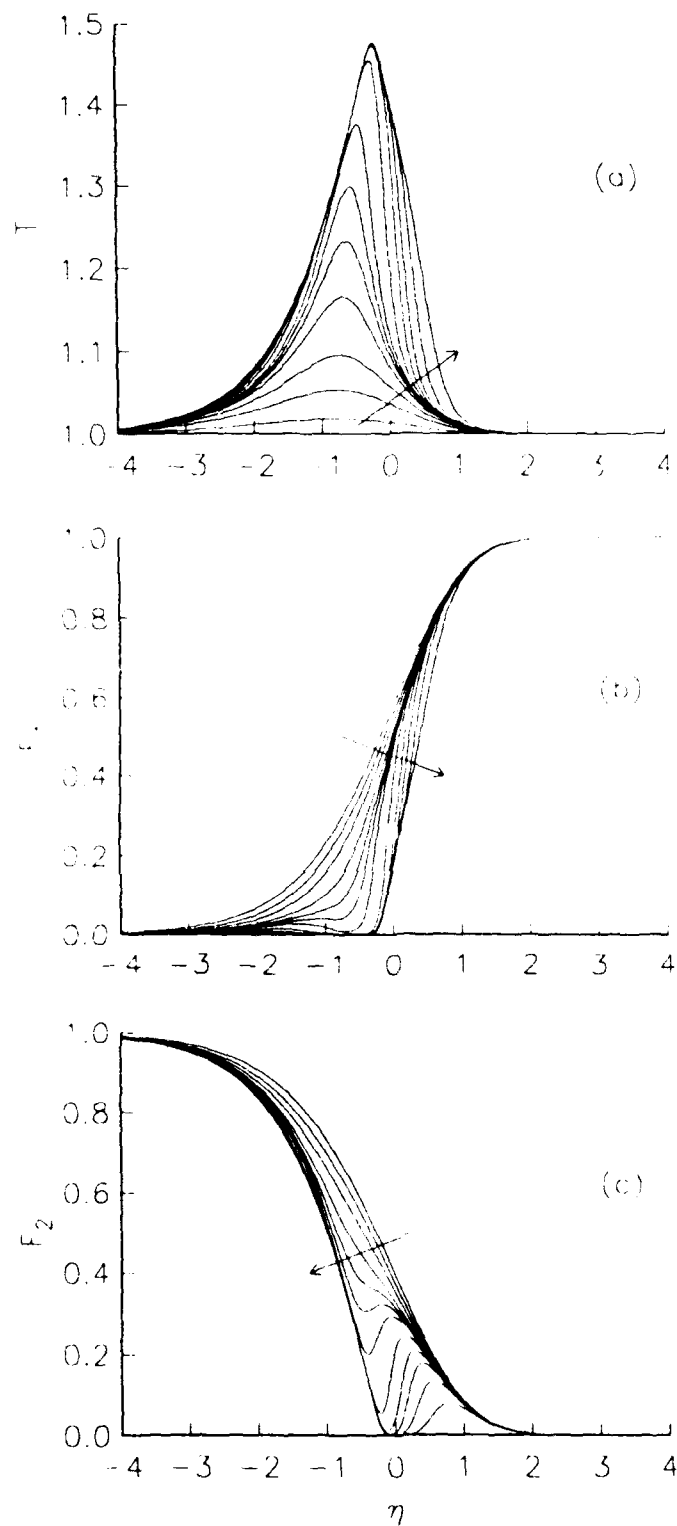


Figure 4. Plot of (a) temperature, (b) F_1 mass fraction, (c) F_2 mass fraction versus η for $M = \beta_U = 0$, $\beta_T = \beta = \phi = 1$, $Ze = 30$. Here, the arrow denotes increasing x , with $x = 1, 2, 2.5, 2.8, 2.9, 2.95, 3, 3.1, 3.2, 3.3, 3.5, 4$.

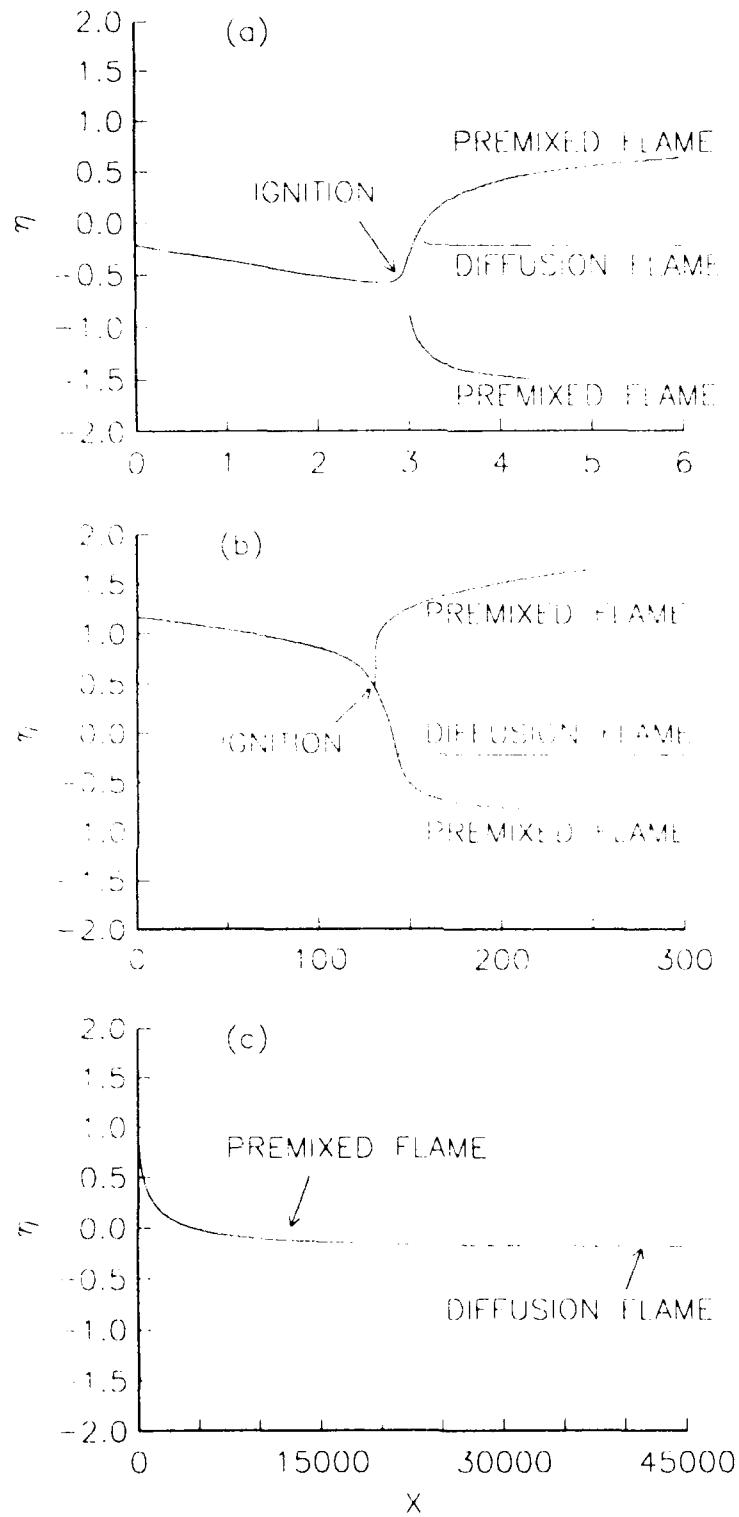


Figure 5. Plot of the loci in the (x, η) plane of the maxima of Ω for $M = \beta_U = 0$, $\phi = 1$, $Ze = 30$, and (a) $\beta_T = \beta = 1$; (b) $\beta_T = 0.5$, $\beta = 1.5$; and (c) $\beta_T = 0.5$, $\beta = 0.4$. Here, $D = \phi e^{Ze} / (\beta Ze)$.

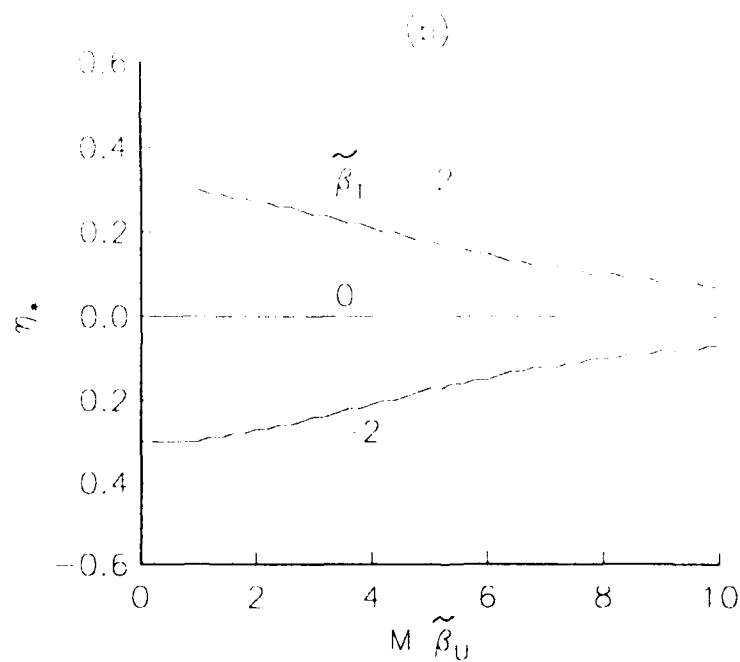
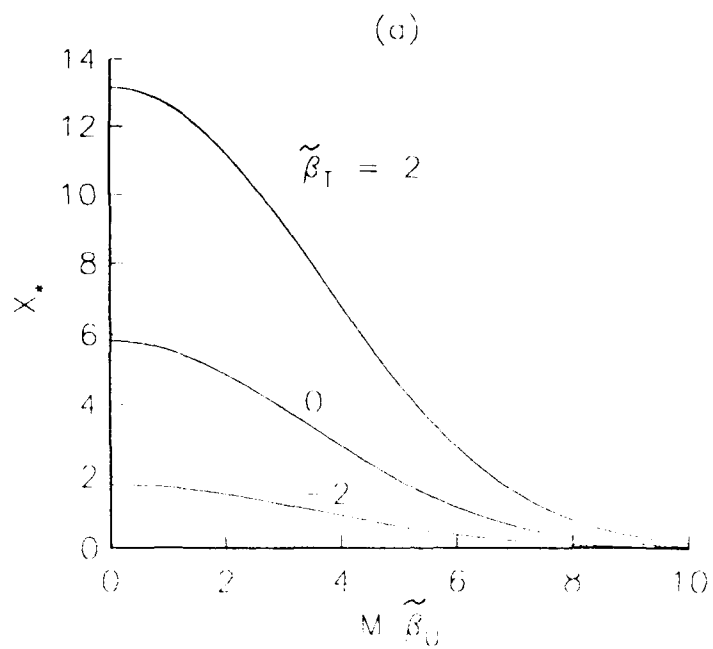


Figure 6. Plot of the ignition location (a) x^* and (b) η^* versus $M \tilde{\beta}_U$ and for $\tilde{\beta}_T = -2, 0, 2$.

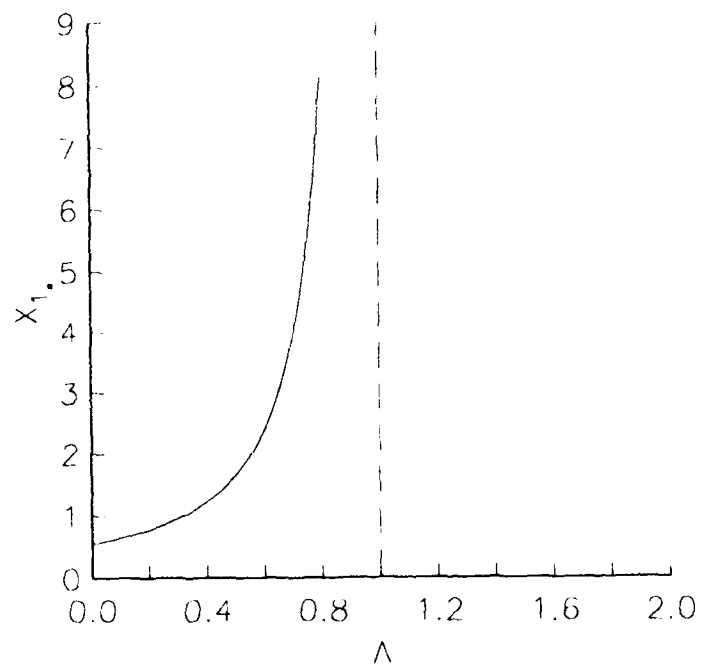


Figure 7. Plot of the ignition location x_1 versus Λ .

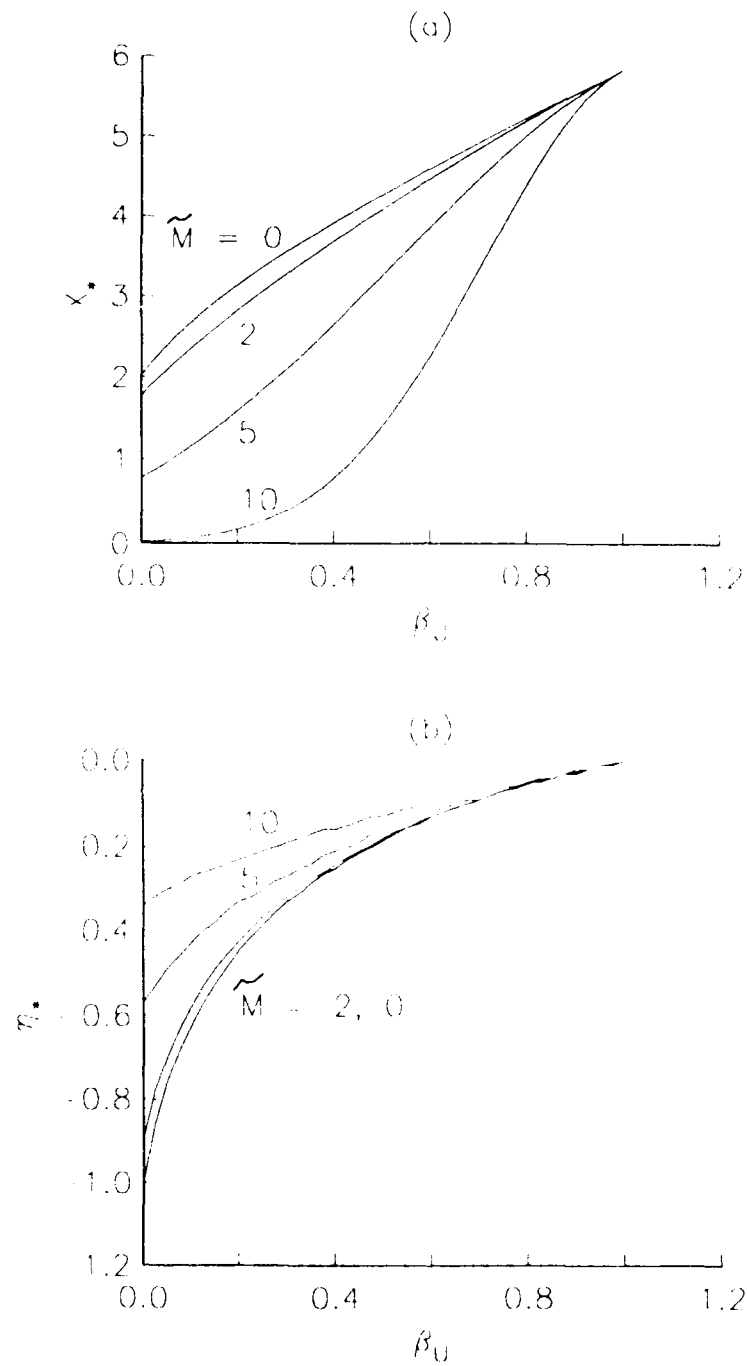


Figure 8. Plot of the ignition location (a) x^* and (b) η^* versus β_U for $\beta_T = 0$ and $\tilde{M} = 0, 2, 5, 10$.

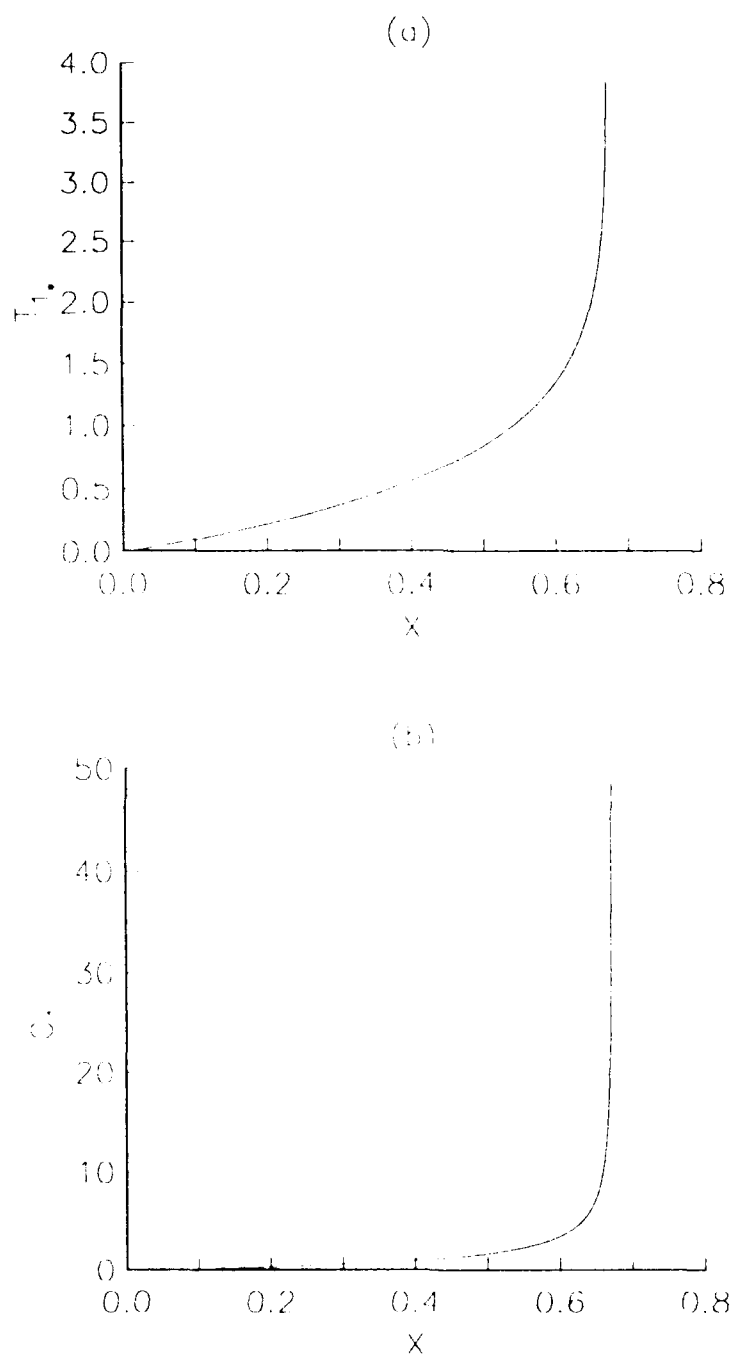


Figure 9. Plot of (a) T_1 and (b) c_1 versus x for $\beta_T = 0.5$, $\beta_U = 0$, and $M = 2$.

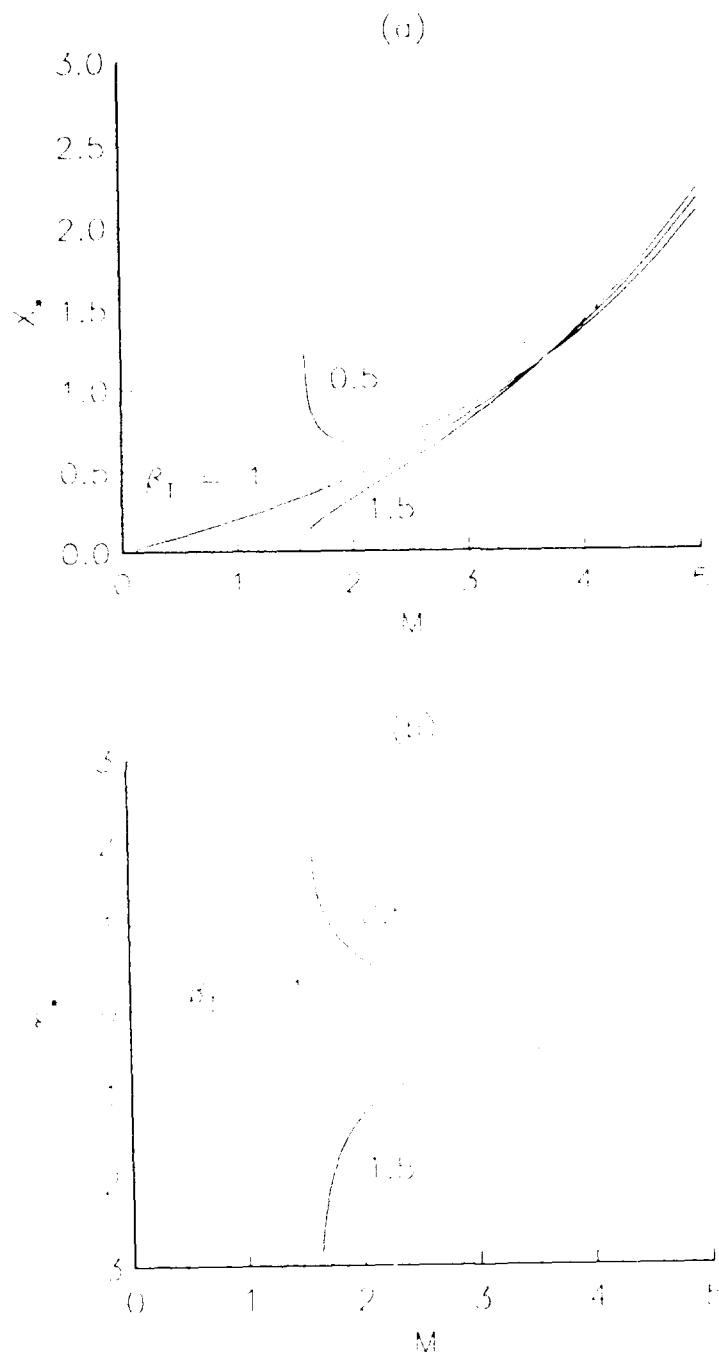


Figure 10. Plot of (a) x_* and (b) η_* versus M for $\beta_U = 0$ and $\beta_F = 0.5, 1.0, 1.5$.

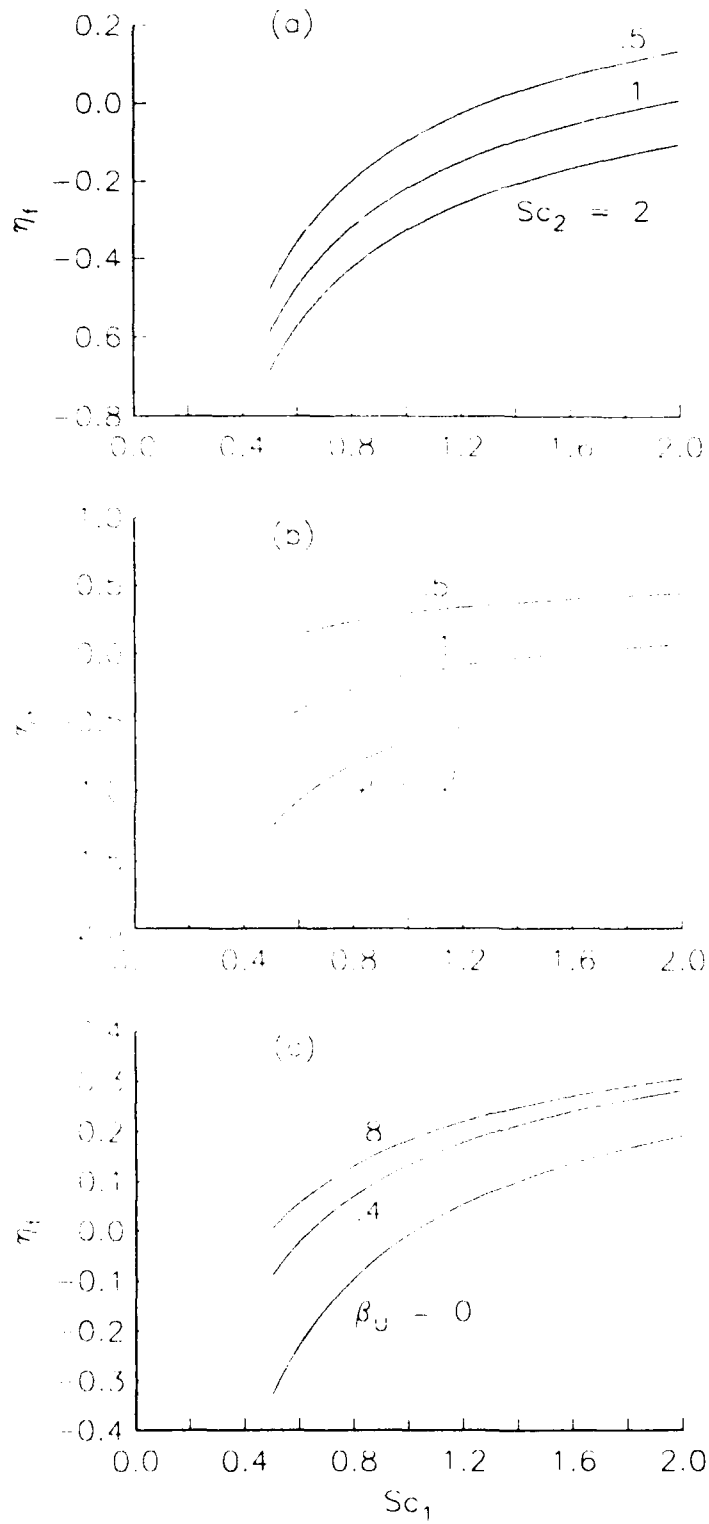


Figure 11. Plot of the flame location η_f versus Sc_1 : (a) $\beta_U = 0$, $\phi = 1$, $Sc_2 = .5, 1, 2$; (b) $\beta_U = 0$, $\phi = .5, 1, 2$, $Sc_2 = .7$; (c) $\beta_U = 0, .4, .8$, $\phi = .8$, $Sc_2 = .7$.